IJARSCT
International Journal of Advanced Research in Science, Communication and Technology
International Open-Access, Double-Blind, Peer-Reviewed, Refereed, Multidisciplinary Online Journal
ISSN: 2581-9429
Volume 6, Issue 4, March 2026
Impact Factor: 8.2

Design and Performance Enhancement of Internal Combustion Engine Connecting Rod Assembly through FEA and Optimization Techniques

[1st]Priyesh Kumar Mishra and [2nd]Dr. Raghvendra Khedle
Department of Heat Power & Thermal Engineering
Technocrat Institute of Technology, Bhopal, India
mishrapriyesh.521@gmail.com

Abstract: *This paper presents a comprehensive design, modeling, and finite element analysis (FEA) of a connecting rod assembly for an internal combustion (IC) engine. The investigation encompasses structural stress analysis, thermal behavior assessment, dynamic load evaluation, and material comparison to identify an optimum configuration that balances mechanical performance with weight efficiency. The performance of the connecting rod was evaluated under cyclic loading conditions, and a comparative analysis was conducted between the existing material (gray cast iron) and the proposed alternative (aluminum alloy 6061) to quantify performance differences under identical loading and boundary conditions. The results show that gray cast iron demonstrates superior heat flux dissipation performance at 50,000 rpm operating conditions, indicating better thermal management potential compared to gray iron under high-speed engine operation. Additionally, the optimized design ensures improved structural integrity and operational efficiency.*

Keywords: Connecting Rod Assembly, Finite Element Analysis (FEA), Thermo-Mechanical Performance, Material Optimization, Dynamic Load Analysis.

I. INTRODUCTION

1.1 Overview

Internal combustion (IC) engines are among the most critical mechanical systems in modern transportation and industrial applications. The engineering community is under increasing pressure to develop compact, lightweight, thermally efficient, and adaptable engines that also reduce pollutant emissions and fuel consumption. Meeting these competing demands necessitates innovative design strategies and rigorous analytical methodologies [1].

To appreciate the progress in IC engine design, one must reflect on more than a century of mechanical innovation is required. The automobile, once a luxury available only to the privileged, has become an indispensable element of modern civilization. The relentless pursuit of performance—faster, lighter, and more fuel-efficient powertrains—has driven engineers to explore advanced materials, computational analysis tools, and optimized geometric configurations[2].

Among the most significant components within an IC engine assembly, as shown in Figure 1, the connecting rod has paramount structural importance. It serves as a mechanical link between the linearly reciprocating piston and the rotating crankshaft, thereby translating combustion-driven linear motion into usable rotational output[3]. Its design must reconcile conflicting mechanical demands: it must withstand enormous compressive and tensile cyclic loads, resist fatigue over hundreds of millions of cycles, and contribute minimally to the overall mass of the engine assembly, as shown in Figure 1.

DOI: 10.48175/IJARSCT-31806

IJARSCT
International Journal of Advanced Research in Science, Communication and Technology
International Open-Access, Double-Blind, Peer-Reviewed, Refereed, Multidisciplinary Online Journal
ISSN: 2581-9429
Volume 6, Issue 4, March 2026
Impact Factor: 8.2

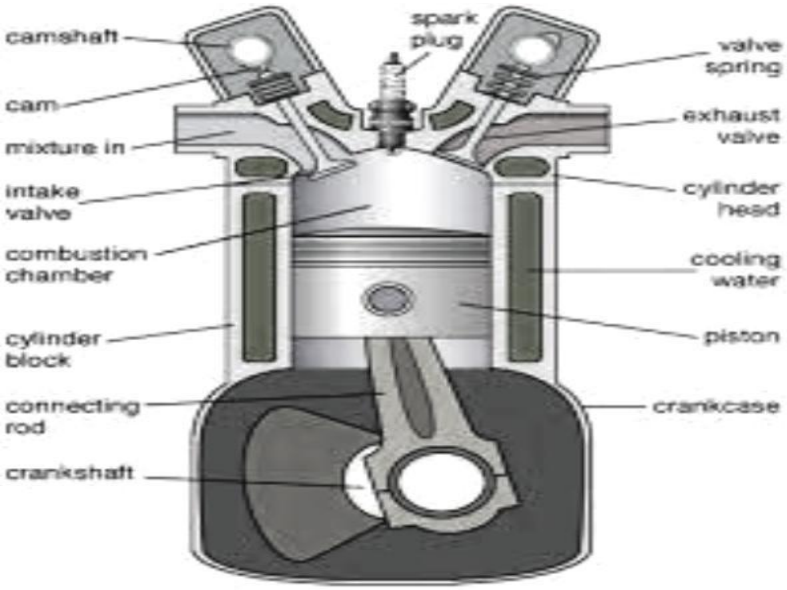

Figure 1 Internal Combustion Engine Assembly

A failure in the connecting rod invariably leads to catastrophic engine damage, making it one of the most consequential components from the standpoint of durability and reliability. The connecting rod was subjected to cyclic loading in the range of 10^8 to 10^9 cycles, alternating between high compressive forces generated by the combustion pressure and significant tensile forces due to inertial loading[3], [4].

This Paper presents a comprehensive design, modeling, and finite element analysis (FEA) of a connecting rod assembly for an IC engine. The investigation encompasses structural stress analysis, thermal behavior assessment, dynamic load evaluation, and material comparison to identify an optimum configuration that balances mechanical performance with weight efficiency.

1.2 Engine Component Failure Statistics

A systematic analysis of seventy automotive component failures reveals that engine-related failures account for approximately 41% of all reported incidents—making them the most prevalent category of component failures. The most common root cause is misuse or operational abuse (29%), followed by inadequate lubrication and assembly errors. These statistics underscore the importance of robust design and analytical verification for engine components such as the connecting rod, piston, and crankshaft.

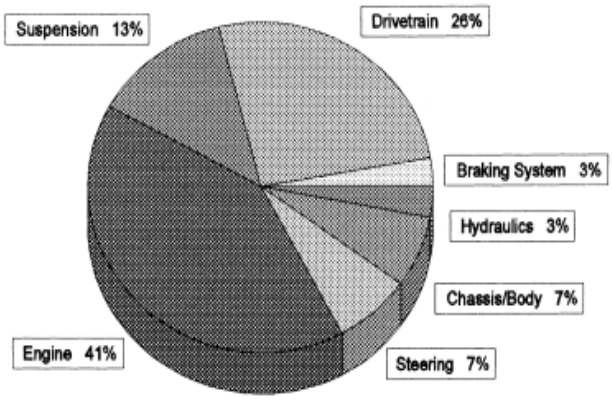

Figure 2 Distribution of Component Failures

IJARSCT
International Journal of Advanced Research in Science, Communication and Technology
International Open-Access, Double-Blind, Peer-Reviewed, Refereed, Multidisciplinary Online Journal
ISSN: 2581-9429
Volume 6, Issue 4, March 2026
Impact Factor: 8.2

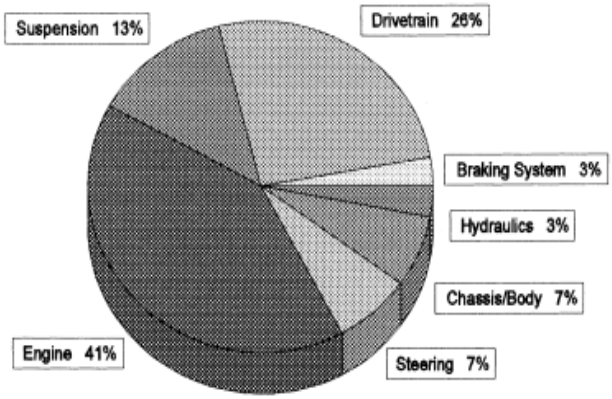

Figure 3 Distribution of Causes of Failure

1.3 Function of the Connecting Rod

The connecting rod transmits the compressive thrust exerted by the piston to the crankshaft, thereby converting reciprocating motion into rotational motion. It consists of three principal structural zones: the small end (piston end), the shank section, and the large end (crankshaft end). Both end pin bores are precision-machined to accommodate appropriate bearing inserts and facilitate smooth rotational contact[5].

One end of the connecting rod is connected to the piston via the gudgeon (wrist) pin, whereas the other end encircles the crankpin and is split into two halves to permit assembly around the crankshaft. The two halves of the big end are secured by precision bolts. The connecting rod is subjected to forces originating from both mass inertia and gas combustion pressure, resulting in complex axial and bending stress states. These stresses arise from eccentricity, crankshaft deflection, and rotating mass forces[6].

II. METHODOLOGY

In the present study, a systematic and simulation-driven methodology was adopted to analyze and optimize the performance of a connecting rod under realistic operating conditions. The overall workflow integrates analytical design, finite element analysis (FEA), and comparative evaluation to ensure both accuracy and engineering reliability.

2.1 Literature Survey

A comprehensive literature review was conducted to understand the state-of-the-art in connecting rod design, material selection, and failure mechanisms. Emphasis was placed on studies involving buckling failure, fatigue behavior, and stress concentration effects. Previous applications of finite element analysis (FEA) in predicting structural performance were critically examined. This step helped identify research gaps and select appropriate analytical and numerical techniques for the present work..

2.2 Design Parameters and Analytical Modeling

The geometric and loading parameters of the connecting rod were defined based on the specifications of the Opra Magnum engine. Key parameters, such as length, cross-sectional dimensions, and applied loads, were determined from the engine operating conditions [7].

The initial sizing of the connecting rod was performed using Rankine's buckling formula, which considers both crushing and buckling effects. The critical load was calculated to ensure that the rod remains safe under compressive forces during engine operation. Analytical calculations were performed to estimate the stress distribution and factor of safety, forming a baseline for comparison with the numerical results.

IJARSCT
International Journal of Advanced Research in Science, Communication and Technology
International Open-Access, Double-Blind, Peer-Reviewed, Refereed, Multidisciplinary Online Journal
ISSN: 2581-9429
Volume 6, Issue 4, March 2026
Impact Factor: 8.2

2.3 CAD Modeling and Pre-processing

A three-dimensional model of the connecting rod was developed using standard CAD tools and subsequently imported into ANSYS Workbench 12.1 for simulation. The geometry was verified for dimensional accuracy and prepared for analysis.

Meshing was performed using appropriate element types to ensure a balance between computational efficiency and solution accuracy. A finer mesh was applied in regions of expected stress concentration, such as the crank and piston ends.

2.4 Boundary Conditions and Finite Element Analysis

Boundary conditions were applied to simulate realistic engine-loading scenarios. The crank end was constrained appropriately, whereas axial loads corresponding to the combustion pressure were applied at the piston end.

Static structural analysis was performed to evaluate the following:

- Von-Mises stress distribution
- Equivalent elastic strain
- Total deformation

Fatigue analysis was conducted to estimate the life cycle of the connecting rod under cyclic loading conditions. The factor of safety was also computed to assess design reliability.

2.5 Validation and Comparative Analysis

The results obtained from the FEA were compared with analytical calculations to validate the accuracy of the simulation model. Key performance indicators such as:

- Von-Mises stress
- Equivalent strain
- Deformation
- Factor of safety
- Fatigue life

were analyzed and correlated. Any deviations were examined to understand the influence of the modeling assumptions and numerical approximations..

2.6 Material Optimization and Design Improvement

Based on the comparative results, different candidate materials were evaluated to identify the optimum material for the connecting rod. The criteria considered were the strength-to-weight ratio, fatigue resistance, and deformation characteristics.

Finally, design improvements were proposed by modifying the geometric parameters and material selection to enhance the performance, reduce the stress concentration, and improve the fatigue life. The optimized design ensures improved structural integrity and operational efficiency of the connecting rod.

III. FAILURE ANALYSIS OF ENGINE COMPONENTS

Identifying the root cause of component failure is a prerequisite for effective preventive design. A structured failure analysis methodology involves four principal steps: (1) visual appearance characterization and morphological description of the failed component, (2) identification of the damaging mechanism responsible for material degradation, (3) enumeration of possible contributing causes, and (4) prescription of corrective engineering actions to prevent recurrence.

The primary sources of thermal stress in engine components arise from inadequate cooling system performance and insufficient or incorrect lubrication. Hydrostatic locking represents an additional, less frequently recognized failure

IJARSCT
International Journal of Advanced Research in Science, Communication and Technology
International Open-Access, Double-Blind, Peer-Reviewed, Refereed, Multidisciplinary Online Journal
ISSN: 2581-9429
Volume 6, Issue 4, March 2026
Impact Factor: 8.2

mode, particularly affecting the connecting rod and piston assembly when water ingress occurs into the combustion chamber through the exhaust system[8].

3.1 Crankshaft Failure

Crankshaft distortion typically occurs due to extreme operating conditions, such as over speeding, lugging, or improper handling prior to installation. A deformed crankshaft imposes excessive loads on the main bearings, with the highest stress concentration at the point of maximum deflection. This leads to accelerated bearing wear and a reduction in oil clearance between the journal and bearing surface, eventually inducing metal-to-metal contact[5], [9].

Additionally, oil clearances near the parting line may reduce to the point where bearing seizure occurs, creating regions of abnormal wear. Improper seating between the bearing back and the housing bore further impedes heat dissipation from the bearing surface, thereby reducing fatigue endurance. Cyclic loading and flexing of the connecting rod can cause the bearing housing bore to become oval-shaped, further compromising bearing performance over time[10]. Figure 4 illustrates surface damage in the form of longitudinal scratches and scoring marks on the main bearing journals of a crankshaft, primarily caused by lubrication failure.

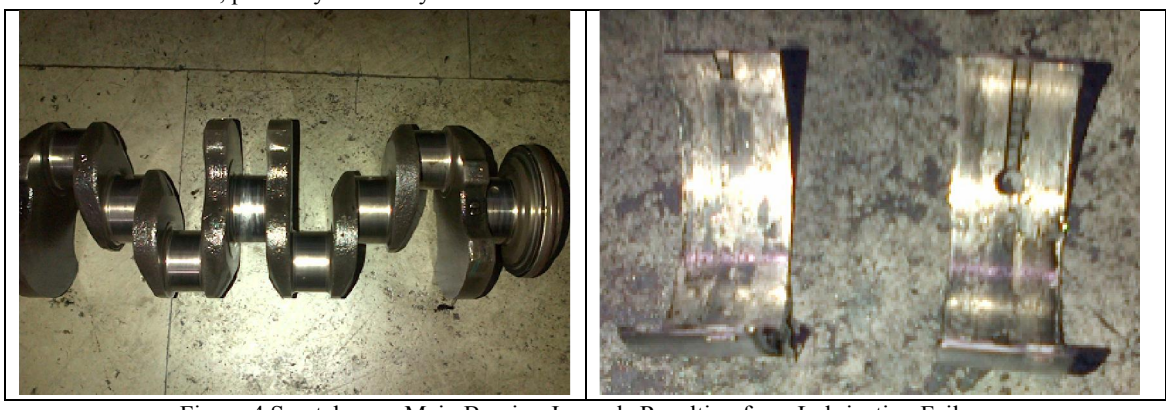

Figure 4 Scratches on Main Bearing Journals Resulting from Lubrication Failure

3.2 Bearing Failure

Bearing failures are predominantly caused by contamination of the lubrication system with dust, abrasive particles, or metallic debris that embeds in the soft Babbitt bearing lining and generates localized high-pressure zones. The major causes of fatigue bearing failure are listed in Table 1. These zones initiate journal-to-bearing contact through a rubbing or grinding mechanism, ultimately leading to progressive coating breakdown and catastrophic failure. External particles partially embedded in the bearing lining may protrude sufficiently to contact the journal, whereas particles trapped between the bearing back and housing bore disrupt thermal conduction from the bearing surface.

Table 1 Major Causes of Fatigue Bearing Failure

Failure Cause	Percentage (%)	Failure Cause	Percentage (%)
Dirt/Contamination	45.4%	Overloading	8.1%
Misassembly	12.8%	Corrosion	3.7%
Misalignment	12.6%	Improper Journal Finish	3.2%
Insufficient Lubrication	11.4%	Other Causes	2.8%

3.3 Connecting Rod Failure

The connecting rod is subjected to a complex multiaxial stress state under service conditions. High cyclic loading in the range of 10^8 to 10^9 cycles alternates between high compressive stresses (due to gas combustion pressure) and

IJARSCT
International Journal of Advanced Research in Science, Communication and Technology
International Open-Access, Double-Blind, Peer-Reviewed, Refereed, Multidisciplinary Online Journal
ISSN: 2581-9429
Volume 6, Issue 4, March 2026
Impact Factor: 8.2

significant tensile stresses (due to inertial loading at top dead center on the exhaust stroke). Therefore, the durability of this component is critically important.

A bent or deformed connecting rod causes misalignment at the bearing bore, resulting in metal-to-metal contact between the bearing shell edge and the journal. This promotes rapid surface wear and can lead to seizing. Cyclic bending of the connecting rod may also cause the bearing bore to elongate, and replacement bearing shells that conform to the distorted bore geometryproduce an out-of-round bearing surface that accelerates subsequent wear.

Hydrostatic locking represents a distinctive failure mode in which water accumulates in the combustion chamber (typically introduced through the exhaust system when a vehicle traverses flooded terrain), as shown in Figure 5. Upon engine startup, the incompressible water column absorbs the full piston force, generating extreme compressive loading in the connecting rod that exceeds its structural capacity, resulting in catastrophic bending failure.

Figure 5 Hydrostatic Lock Effect on Connecting Rod

3.4 Piston Failure

The piston assembly, comprising the piston, piston pin, and associated bearing system, is a dynamically sensitive subsystem in an engine. The piston crown forms the bottom boundary of the combustion chamber and is exposed to extreme thermal and pressure cycles. Stress concentration effects at the piston pin boss and crown perimeter are primary initiators of fatigue cracking. Piston seizure occurs when the lubricating oil film between the piston skirt and cylinder bore breaks down, typically due to overheating caused by cooling system failure or oil starvation, as shown in Figure 6.

Figure 6 Worn Piston due to Thermal Overloading and Oil Film Breakdown

IJARSCT
International Journal of Advanced Research in Science, Communication and Technology
International Open-Access, Double-Blind, Peer-Reviewed, Refereed, Multidisciplinary Online Journal
ISSN: 2581-9429
Volume 6, Issue 4, March 2026
Impact Factor: 8.2

3.5 Engine Cooling and Lubrication System Failure

Combustion gas temperatures within engine cylinders can reach 2200°C or higher during peak pressure cycles. The cooling system is specifically designed to maintain cylinder wall temperatures below 260°C under all operating conditions. Higher sustained wall temperatures degrade the lubricating oil viscosity and film strength, leading to metal-to-metal contact and accelerated wear.

Proper lubrication requires the correct oil viscosity specification, a fully functional oil pump, adequate oil gallery flow capacity, and a clean oil supply. During cold engine starts, operators should avoid high-speed acceleration for approximately one minute to allow the oil pump to establish full pressure throughout the lubrication circuit. Failure to observe this precaution results in momentary dry contact at critical bearing surfaces..

IV. DESIGN OF CONNECTING ROD

The connecting rod consists of a long shank section, a small end (piston end), and a large end (crankshaft end). The cross-sectional geometry of the shank may be rectangular, circular, tubular, I-section, or H-section. Circular sections are typically employed in low-speed engines, whereas I-sections are preferred for high-speed applications owing to their superior buckling resistance relative to the material weight.

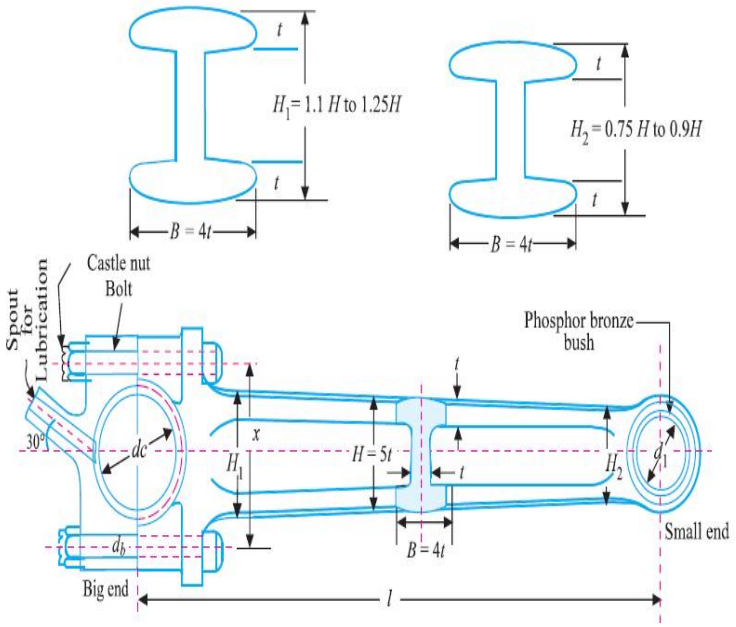

Figure 7 Sectional View of Connecting Rod with Key Geometric Parameters

IJARSCT
International Journal of Advanced Research in Science, Communication and Technology
International Open-Access, Double-Blind, Peer-Reviewed, Refereed, Multidisciplinary Online Journal
ISSN: 2581-9429
Volume 6, Issue 4, March 2026
Impact Factor: 8.2

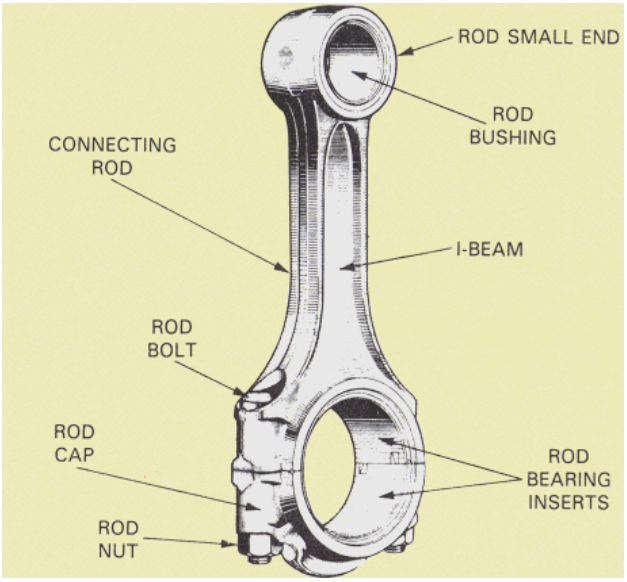

Figure 8 Three-Dimensional View of Connecting Rod Assembly

The connecting rod length (l) is defined by the ratio l/r, where r is the crank radius. Shorter connecting rods (low l/r ratio) increase the angularity of the rod relative to the cylinder axis, elevating the side force exerted by the piston on the cylinder liner and thereby accelerating liner wear. Conversely, longer connecting rods reduce angularity and side force but increase the overall engine height. A compromise value of l/r = 4 to 5 is generally adopted in practice.

4.1 Engine Specifications (Opra Magnum Engine)

The following engine specifications were used for all connecting rod design calculations:

Table 2 Design Specifications — Opra Magnum Engine

Parameter	Value
Engine Type	Four-cylinder, Inline, SOHC
Engine Speed (N)	3000 rpm
Maximum Gas Pressure (p)	3.15 N/mm²
Bore Diameter (D)	83 mm
Reciprocating Mass (m_R)	2.25 kg
Connecting Rod Length (l)	380 mm
Stroke	92 mm
Compression Ratio	17.5 : 1
Factor of Safety (F.S.)	6

4.2 Design of I-Section Connecting Rod

An I-section profile is selected for the connecting rod shank with the following geometric proportions:

- Flange and web thickness = t
- Section width, B = 4t
- Section depth/height, H = 5t

DOI: 10.48175/IJARSCT-31806

IJARSCT
International Journal of Advanced Research in Science, Communication and Technology
International Open-Access, Double-Blind, Peer-Reviewed, Refereed, Multidisciplinary Online Journal
ISSN: 2581-9429
Volume 6, Issue 4, March 2026
Impact Factor: 8.2

V. FINITE ELEMENT ANALYSIS — THEORY AND METHODOLOGY

5.1 Introduction to the Finite Element Method

The finite element method (FEM) is a numerical computational technique for solving engineering and physical science problems involving complex geometries, boundary conditions, and material properties that cannot be addressed analytically. In FEM, a continuum body or structure is discretized into a finite number of smaller subregions called finite elements, which are interconnected at discrete points known as nodes. The behavior of each element is characterized by its constitutive equations, which are assembled into a global system and solved simultaneously to obtain a solution for the entire domain.

In contrast to solving the governing differential equations for the entire body in a single operation, the FEM formulates equations element by element and assembles them into a global system. This approach provides accurate solutions for structural mechanics, fluid mechanics, heat transfer, mass transport, and electromagnetic field problems, including complex multiaxial stress states characteristic of IC engine components.

5.2 Classification of Finite Element Problems

5.2.1 Structural Problems

In structural FEA, the nodal displacements are the primary unknowns. Once the displacement field is established, the element stresses and strains are computed using constitutive relationships and strain–displacement equations. Applications include static stress analysis, modal analysis, buckling prediction, and fatigue life estimation.

5.2.2 Non-Structural Problems

Nonstructural FEA problems involve thermal, fluid, or electromagnetic field quantities as the primary nodal unknowns. Temperature distributions and heat flux values were obtained from thermal analyses, whereas pressure and velocity fields were extracted from fluid flow simulations. Both categories can be coupled in multiphysics analyses, as is the case in the thermal–structural analysis of engine components.

5.3 Application Areas of FEM in Mechanical Engineering

The finite element method has become indispensable across virtually all branches of mechanical and structural engineering. In the automotive sector, FEA enables engineers to evaluate component integrity under complex loading scenarios without expensive physical testing at every design iteration. Key application areas include:

- Structural strength and rigidity analysis of engine components
- Fluid-structure interaction analysis for cooling passages
- Shock and impact analysis (crash simulations)
- Acoustic and noise-vibration-harshness (NVH) analysis
- Steady-state and transient thermal analysis
- Modal (natural frequency) and harmonic vibration analysis
- Buckling stability analysis under compressive loading
- Electromagnetic field analysis for sensors and actuators
- Coupled thermo-structural analysis for high-temperature components

5.4 Distinction between FEM and FEA

FEM refers to the underlying mathematical framework—the variational formulation, element type selection, polynomial interpolation functions, and assembly procedures that constitute the theoretical basis of the method. FEA, by contrast, is the practical application of FEM to a specific engineering analysis problem, incorporating element type selection (e.g., tetrahedral, hexahedral), mesh generation strategies, boundary condition specification, solver selection, and result post-processing. Both terms are frequently used interchangeably in industrial practice.

IJARSCT
International Journal of Advanced Research in Science, Communication and Technology
International Open-Access, Double-Blind, Peer-Reviewed, Refereed, Multidisciplinary Online Journal
ISSN: 2581-9429
Volume 6, Issue 4, March 2026
Impact Factor: 8.2

5.5 Design Analysis Workflow Using FEA

5.5.1 Design Validation

FEA can verify that a proposed design satisfies structural performance criteria before physical prototypes are manufactured, substantially reducing development cost and time-to-market. This is particularly valuable for engine components where physical testing requires dynamometer facilities and extended run-in periods.

5.5.2 Design Optimization

Parametric FEA studies enable systematic variation of geometric or material parameters to identify configurations that minimize stress concentration, weight, or manufacturing cost while maintaining required structural integrity. This capability is exploited in the present study for connecting rod cross-sectional geometry and material selection.

5.6 ANSYS Workbench 12.1 Overview

ANSYS is a large-scale, multipurpose finite element analysis software package capable of solving a broad spectrum of engineering problems. The ANSYS environment integrates capabilities for static and dynamic structural analysis, steady-state and transient thermal analysis, modal and buckling analysis, electromagnetic analysis, and coupled multi-physics simulations. Advanced features include contact mechanics, large deformation, hyper-elasticity, creep, plasticity, and radiation heat transfer.

The ANSYS Workbench platform provides a project-based analysis environment with intuitive drag-and-drop workflows, integrated geometry modeling and mesh generation tools, and comprehensive post-processing visualization capabilities including contour plots, vector plots, and animation sequences.

VI. RESULTS AND DISCUSSION

6.1 Comparison of Gray Cast Iron vs. Aluminum Alloy 6061

A focused comparative analysis was conducted between the existing material (gray cast iron) and the proposed alternative (aluminum alloy 6061) to quantify performance differences under identical loading and boundary conditions. The following figures present simulation results for both materials across static structural, thermal, and explicit dynamic analysis categories.

6.1.1 Static Structural Analysis — Aluminum Alloy 6061

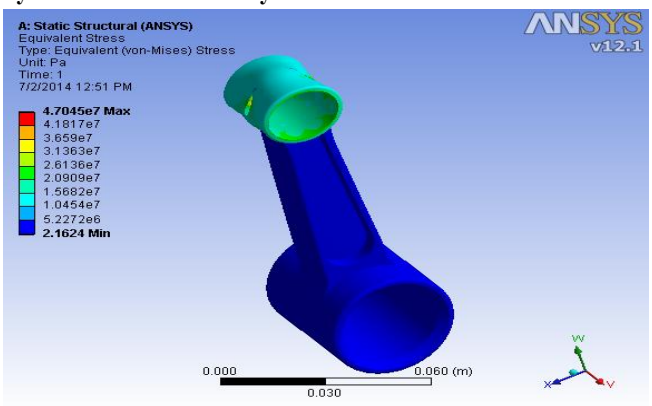

Figure 9 Von-Mises Stress Distribution — Aluminum Alloy 6061

Quantitative Results Tables — Gray Cast Iron vs. Aluminum Alloy 6061

IJARSCT
International Journal of Advanced Research in Science, Communication and Technology
International Open-Access, Double-Blind, Peer-Reviewed, Refereed, Multidisciplinary Online Journal
ISSN: 2581-9429
Volume 6, Issue 4, March 2026
Impact Factor: 8.2

Table 3 Von-Mises Stress — Gray Cast Iron vs. Aluminum Alloy 6061

Material	Von-Mises Stresses	Condition	Value (Pa)
Gray Cast Iron	Von-Mises Stress	MAX	4.70×10^7
Aluminum Alloy 6061	Von-Mises Stress	MAX	4.70×10^7
Gray Cast Iron	Von-Mises Stress	MIN	2.16×10^7
Aluminum Alloy 6061	Von-Mises Stress	MIN	2.16×10^7

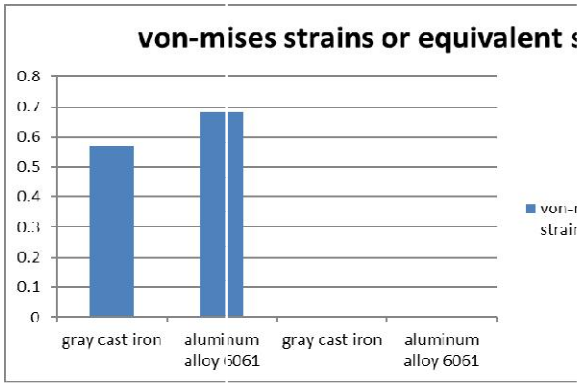

Figure 10 Von-Mises Equivalent Strains Comparison

Table 4 Von-Mises Equivalent Strains — Gray Cast Iron vs. Aluminum Alloy 6061

Material	Condition	Equiv. Strain (m/m)
Gray Cast Iron	MAX	0.5668
Aluminum Alloy 6061	MAX	0.68181
Gray Cast Iron	MIN	2.61×10^{-8}
Aluminum Alloy 6061	MIN	3.13×10^{-8}

TABLE 5 Total Deformation — Gray Cast Iron vs. Aluminum Alloy 6061

Material	Condition	Total Deformation (m)
Gray Cast Iron	MAX	0.0031989
Aluminum Alloy 6061	MAX	0.003848
Gray Cast Iron	MIN	0
Aluminum Alloy 6061	MIN	0

DOI: 10.48175/IJARSCT-31806

IJARSCT
International Journal of Advanced Research in Science, Communication and Technology
International Open-Access, Double-Blind, Peer-Reviewed, Refereed, Multidisciplinary Online Journal
ISSN: 2581-9429
Volume 6, Issue 4, March 2026
Impact Factor: 8.2

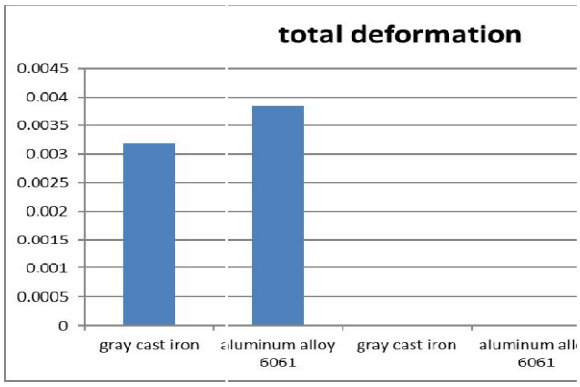

Chart 1 Total Deformation Comparison

Table 6 Factor of Safety — Gray Cast Iron vs. Aluminum Alloy 6061

Material	Condition	Factor of Safety
Gray Cast Iron	MAX	15
Aluminum Alloy 6061	MAX	15
Gray Cast Iron	MIN	1.8323
Aluminum Alloy 6061	MIN	1.8435

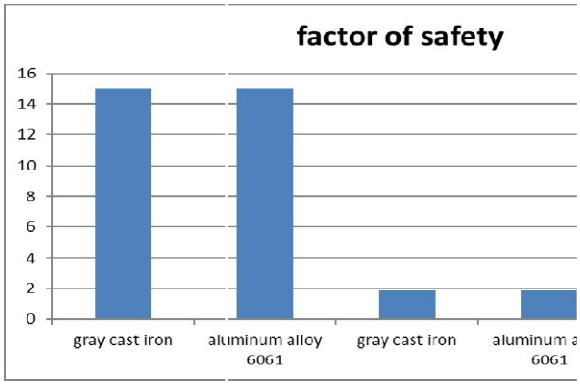

Chart 2 Factor of Safety Comparison

Table 7 Thermal Analysis — Temperature Distribution

Material	Condition	Temperature (K)
Gray Cast Iron	MAX	1.07×10^3
Aluminum Alloy 6061	MAX	1.07×10^3
Gray Cast Iron	MIN	1.07×10^3
Aluminum Alloy 6061	MIN	1.07×10^3

DOI: 10.48175/IJARSCT-31806

IJARSCT
International Journal of Advanced Research in Science, Communication and Technology
International Open-Access, Double-Blind, Peer-Reviewed, Refereed, Multidisciplinary Online Journal
ISSN: 2581-9429
Volume 6, Issue 4, March 2026
Impact Factor: 8.2

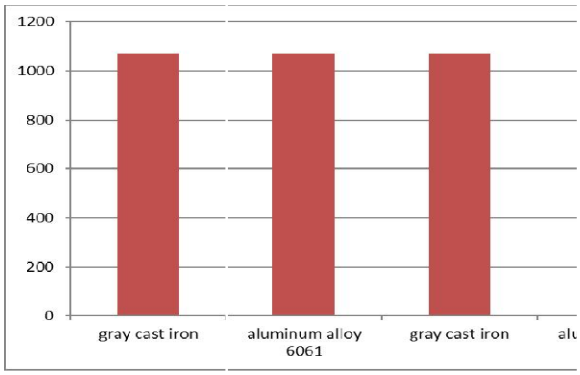

Chart 3 Temperature Comparison — Gray Cast Iron vs. Aluminum Alloy 6061

Thermal analysis results confirm that the surface temperature distribution is essentially identical for both gray cast iron and aluminum alloy 6061 under the applied boundary conditions, indicating no thermal advantage of one material over the other at the prescribed operating temperature.

Table 8 Total Heat Flux Results

Material	Condition	Heat Flux (W/m²)
Gray Cast Iron	MAX	1.33×10^{4}
Aluminum Alloy 6061	MAX	1.23×10^{4}
Gray Cast Iron	MIN	2.34×10^{-8}
Aluminum Alloy 6061	MIN	4.34×10^{-8}

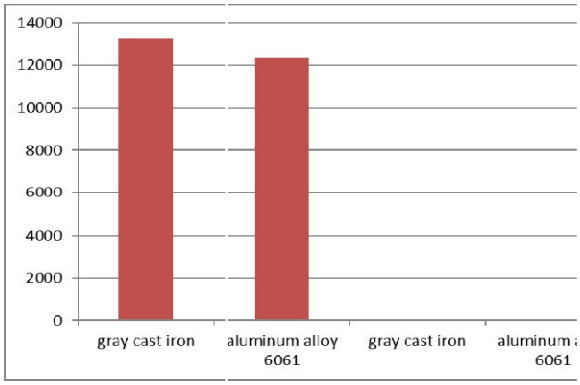

Chart 4 Total Heat Flux Comparison

Aluminum alloy 6061 demonstrates superior heat flux dissipation performance at 50,000 rpm operating conditions, suggesting better thermal management potential compared to gray cast iron under high-speed engine operation.

Table 9 Directional Heat Flux Results

Material	Condition	Dir. Heat Flux (W/m²)
Gray Cast Iron	MAX	1.15×10^{4}
Aluminum Alloy 6061	MAX	9.49×10^{3}
Gray Cast Iron	MIN	-1.11×10^{4}
Aluminum Alloy 6061	MIN	-1.08×10^{4}

DOI: 10.48175/IJARSCT-31806

IJARSCT
International Journal of Advanced Research in Science, Communication and Technology
International Open-Access, Double-Blind, Peer-Reviewed, Refereed, Multidisciplinary Online Journal
ISSN: 2581-9429
Volume 6, Issue 4, March 2026
Impact Factor: 8.2

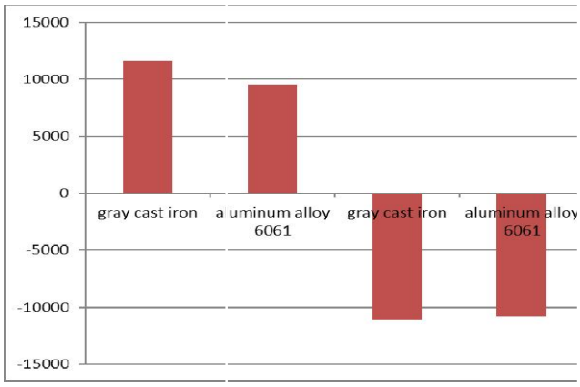

Chart 5 Directional Heat Flux Comparison

6.3 Dynamic Stress Analysis — Aluminum Alloy 6061

Table 10 Explicit Dynamic Stress Analysis — Aluminum Alloy 6061 Connecting Rod

Analysis Type	Condition	Value (Pa)
Von-Mises Stresses	MAX	4.70×10^7
Von-Mises Stresses	MIN	2.16×10^7
Equivalent Elastic Strain	MAX	4.70×10^7
Total Deformation	MAX	4.70×10^7

6.4 Weight Reduction Analysis

Table 11 Mass Comparison — Gray Cast Iron vs. Aluminum Alloy 6061

Material	Mass of Connecting Rod (kg)
Gray Cast Iron	0.29054 kg
Aluminum Alloy 6061	0.10971 kg

The weight reduction achieved by substituting gray cast iron with aluminum alloy 6061 as shown in Table 11 for the same connecting rod geometry is computed as follows:

$$\% \text{ Weight Reduction} = [(0.29054 - 0.10971) / 0.29054] \times 100 = 62.2\%$$

This substantial 62.2% reduction in connecting rod mass represents a significant engineering achievement. Reduced reciprocating mass directly lowers inertial forces at high engine speeds, enabling higher RPM operation, reduced bearing loads, lower vibration levels, and improved fuel efficiency due to decreased internal friction work.

REFERENCES

[1]. G. Zhu, F. F. Teixeira, and P. Loh, "Parametric FEM-Based Analysis on Adaptive Vein Morphology of Dragonfly Wings Toward Material Efficiency," Biomimetics, vol. 10, no. 12, p. 799, Nov. 2025, doi: 10.3390/biomimetics10120799.

[2]. R. Y. Dahham, H. Wei, and J. Pan, "Improving Thermal Efficiency of Internal Combustion Engines: Recent Progress and Remaining Challenges," Energies, vol. 15, no. 17, p. 6222, Aug. 2022, doi: 10.3390/en15176222

[3]. A Chmielowiec, W. Woś, and J. Czyżewski, "Numerical Analysis of Inertia Forces in the Connecting Rod and Their Impact on Stress Formation.," Materials, vol. 18, no. 6, p. 1385, Mar. 2025, doi: 10.3390/ma18061385.

[4]. Z. Liu, Z. He, L. Tu, X. Liu, H. Liu, and J. Liang, "A fatigue reliability assessment approach for wind turbine blades based on continuous time Bayesian network and FEA," Quality & Reliability Eng, vol. 39, no. 5, pp. 1603–1621, Jan. 2023, doi: 10.1002/qre.3262.

IJARSCT
International Journal of Advanced Research in Science, Communication and Technology
International Open-Access, Double-Blind, Peer-Reviewed, Refereed, Multidisciplinary Online Journal
ISSN: 2581-9429
Volume 6, Issue 4, March 2026
Impact Factor: 8.2

[5]. Y. Bi et al., "Influence of the Pre-Compensation Profile on the Dynamics and Friction Performance of the Piston Skirt–Cylinder Liner System in a Diesel Engine," Energies, vol. 18, no. 21, p. 5833, Nov. 2025, doi: 10.3390/en18215833.

[6]. P. S. Ranjit et al., "Comprehensive Comparative Study of the Durability Wear Assessment of a Diesel Engine Fuelled with Jatropha Seed Oil and Diesel Fuel and Its Troubleshooting and Scheduled Maintenance.," ACS Omega, vol. 9, no. 43, pp. 43331–43352, Oct. 2024, doi: 10.1021/acsomega.4c00204.

[7]. X. Xu et al., "Adjustable Ultra-Light Mechanical Negative Poisson's Ratio Metamaterials with Multi-Level Dynamic Crushing Effects.," Small, vol. 20, no. 43, July 2024, doi: 10.1002/smll.202403082.

[8]. G. Cicalese, F. Berni, S. Fontanesi, A. D'Adamo, and E. Andreoli, "A Comprehensive CFD-CHT Methodology for the Characterization of a Diesel Engine: from the Heat Transfer Prediction to the Thermal Field Evaluation," Society Of Automotive Engineers, Oct. 2017. doi: 10.4271/2017-01-2196.

[9]. C. Laubichler, C. Kiesling, M. Marques Da Silva, A. Wimmer, and G. Hager, "Data-Driven Sliding Bearing Temperature Model for Condition Monitoring in Internal Combustion Engines," Lubricants, vol. 10, no. 5, p. 103, May 2022, doi: 10.3390/lubricants10050103.

[10]. L. Bai, J. Sun, P. Zhang, and Z. A. Khan, "Friction Behavior of a Textured Surface against Several Materials under Dry and Lubricated Conditions," Materials, vol. 14, no. 18, p. 5228, Sept. 2021, doi: 10.3390/ma14185228